

## Role of Cracks in Progressive Permeability Reduction During Flow of Heated Aqueous Fluids Through Granite

PETER J. VAUGHAN,<sup>1</sup> DIANE E. MOORE, CAROLYN A. MORROW, AND JAMES D. BYERLEE

*U.S. Geological Survey, Menlo Park, California*

Permeability was measured continuously during an experiment in which a heated, aqueous fluid was pumped through a cylindrical sample of Westerly Granite. Fluid flowed radially outward from an axial borehole down a temperature gradient to the outer edge of the sample. The fluid temperature in the borehole was maintained at 300°C, while a pore pressure difference of 0.5 MPa provided the driving force for fluid flow. Permeability decreased by a factor of 25 during the 2-week experiment. Scanning electron microscope examination of this altered sample indicates that about half of the grain boundaries involving quartz are cracked or were cracked at some time during the experiment and now contain a filling material. Grain boundaries between the two feldspars are closed in the starting material and in all areas of the altered sample that were examined. Intragranular cracks in all three major minerals are open in the starting material. These observations suggest that initially, the quartz forms a more effective fluid pathway than do the feldspars. About half of the intragranular cracks near the borehole are open, whereas the other half contain a massive deposit which is either Si-rich or Ca-rich. In most cracks at the outer edge of the altered sample a Si-rich filling is present. In crack intersections in this area the filling has a platy texture. At several times during the experiment the discharged fluids were sampled and chemically analyzed. The silica content of fluids passing through the sample was calculated as a function of radius, using rate equations for the dissolution and precipitation of silica. The calculated silica concentrations for the discharged fluids are approximately in agreement with measured values. A separate calculation of the reduction of crack porosity due to uniform dissolution and reprecipitation of quartz indicates that these processes caused a maximum of 10% crack porosity change for an experiment with a borehole temperature of 300°C. Assuming that reprecipitation of quartz was homogeneous, this porosity change corresponds to a permeability reduction of 27%, whereas the observed value was 96%. Therefore other processes besides the simple homogeneous precipitation of a layer of quartz must be operating to reduce permeability. Four possible processes are (1) nonhomogeneous precipitation, (2) precipitation in critical narrow places in cracks, (3) precipitation of other minerals in addition to quartz, and (4) crack healing.

### INTRODUCTION

Several studies have demonstrated that the permeability of granite decreases substantially with time during experiments in which a heated aqueous fluid was passed through the rock down an applied temperature gradient [Morrow *et al.*, 1981; Moore *et al.*, 1983]. As an example, permeability decreased by a factor of 25 during an experiment of this type on Westerly Granite which lasted for 2 weeks (W300 [Moore *et al.*, 1983]). In an experiment on Barre Granite at 100°C in which an axial load was applied to the sample, permeability decreased with time even though the sample was increasingly dilatant [Kranz and Blacic, 1984]. The purpose of the present work is to provide some insight into the physical characteristics of granite which are responsible both for its initial permeability and for the changes in permeability with time. To accomplish this goal, we examined one of the intact Westerly Granite samples (NWD 2200, called W300 by Moore *et al.* [1983]) utilizing an optical microscope and a scanning electron microscope (SEM). Westerly Granite was chosen as a sample material because information regarding its physical properties and microstructures, including the statistical distribution of crack dimensions [Sprunt and Brace, 1974; Hadley, 1976], is readily available. This partic-

ular experimental sample was chosen because the permeability reduction observed was representative of that found in the intact granite samples.

In an earlier permeability study on Westerly Granite, Brace *et al.* [1968] noted a decrease in permeability with increasing effective pressure (defined here as confining pressure minus pore pressure). The closure of low aspect ratio cracks was believed to be responsible for the observed decrease in permeability [Brace *et al.*, 1968]. Aspect ratio is defined as the ratio of the minimum to the maximum opening of a crack. Further studies have demonstrated conclusively that low aspect ratio cracks control the permeability of Westerly Granite [Brace, 1977; Hadley, 1976]. The high aspect ratio cracks (pores) in granites are isolated and do not form continuous fluid pathways [Montgomery and Brace, 1975]. Thus, in looking for an explanation of the large permeability reduction observed during experiment NWD 2200 of Moore *et al.* [1983], it seems worthwhile to examine the low aspect ratio cracks.

The open cracks in the starting Westerly material were probably generated during the unroofing of the granite, and the most important factor controlling crack opening during this process is the reduction in temperature [Bruner, 1984]. As effective confining pressure was raised during the NWD 2200 permeability experiment [Moore *et al.*, 1983], the open, low aspect ratio cracks tended to close. Most low aspect ratio cracks in granites become closed at an effective confining pressure somewhere in the range of 50 MPa [Simmons and Caruso, 1983] to 100–200 MPa [Warren, 1977]. Because the effective pressure in experiment NWD 2200 was 40 MPa,

<sup>1</sup> Now at Department of Computer Sciences, State University of New York at Plattsburgh.

This paper is not subject to U.S. copyright. Published in 1986 by the American Geophysical Union.

Paper number 5B5632.

TABLE 1. Experimental Conditions and Permeabilities

	NWD 2100	NWD 2200
Confining pressure, MPa	30	60
Pore pressure, MPa	10	20
Pore pressure difference,* MPa	0.5	0.5
Temperature		
Borehole, °C	250	300
Jacket, °C	84	92
Duration of run, days	12	13
Initial permeability, m <sup>2</sup>	7.30E-19	2.40E-19
Final permeability, m <sup>2</sup>	4.6E-20	9.2E-21

Read 7.30E-19 as  $7.30 \times 10^{-19}$ .

\* As measured between the borehole and the jacket of the sample.

some fraction of the original set of low aspect ratio cracks should have remained open. However, the calculations of Bruner [1984] would seem to suggest that the increased temperatures also caused cracks to close during this permeability experiment. Furthermore, substantial radial temperature gradients introduced thermal stresses which probably contributed to crack closure in the region near the borehole.

The reductions in permeability observed during the experiments of Moore *et al.* [1983] were attributed to filling of cracks which comprised the fluid pathways by material that had been dissolved in other regions of the sample where the temperature was higher [Morrow *et al.*, 1981; Moore *et al.*, 1983]. Based on SEM (scanning electron microscope) observations, they identified silica and zeolitic fibers lining fracture surfaces in a sample that had been fractured prior to testing. Morrow *et al.* [1981] concluded that the deposition of these materials was the probable cause of the permeability reduction. The transport and precipitation of material in cracks over grain scale and larger distances are called crack sealing [Smith and Evans, 1984].

A different potential mechanism for permeability reduction is crack healing, as opposed to crack sealing. Crack healing occurs by dissolution and reprecipitation of minerals on a local scale within cracks, such that the precipitated material is in crystallographic continuity with the surrounding grain [Smith and Evans, 1984]. Smith and Evans [1984] conducted annealing experiments on a fractured pure quartz sample to study crack healing under hydrothermal conditions. Their results emphasized the importance of a pore fluid to the crack healing process, because crack healing occurred at 400°C in the presence of a pore fluid but it did not occur at 600°C in the absence of such a fluid. A significant temperature dependence for the crack healing process was also demonstrated by experiments with  $p_{\text{fluid}} = p_{\text{total}}$  at 200°C [Smith and Evans, 1984]; crack healing at these conditions did not occur for experimental times of up to 2 days and original surface structures of cracks, including surface steps and hackle marks, were still present. Based on Smith and Evans' [1984] work, crack healing would only be important for those regions of the samples that were held at temperatures greater than 200°C. However, the conditions of fluid flow and nonhydrostatic stress that were obtained in our samples might possibly have an effect on crack healing.

The composition of fluids discharged from the samples subjected to a flow of heated fluid has been determined during the permeability experiments [Moore *et al.*, 1983]. The discharged fluids are end products of a complex series of chemical interactions which have occurred at different temperatures during the transport of the fluids through the rock.

Analyses of the discharged fluid compositions using the SOLMNEQ speciation-solubility program [Kharaka and Barnes, 1973] indicate that the discharged fluids are supersaturated with respect to several different minerals. Some of these minerals, such as quartz, are present in the starting material. Thus precipitation of quartz could occur at least near the outer edge of the sample. However, this would not rule out the possibility of precipitation of some other silicate instead because the discharged fluids are not in equilibrium with the rock and equilibrium thermodynamics cannot be applied to deducing the composition of the fluids within the sample. The alternative is to use kinetic models of the reactions in the sample. However, the rate constants for many potential reactions, even simple dissolution-precipitation, are not available.

The major goal of the present work is to examine the low aspect ratio cracks in the Westerly sample to determine the changes that have occurred during the experiment. Such observations could provide further information regarding the mechanism of permeability reduction. For example, SEM studies of cracks in different parts of the sample might reveal where crack-sealing or crack-healing processes had occurred. Furthermore, the composition of material contained in the low aspect ratio cracks may be determined, in a qualitative sense, by energy dispersive X ray analysis (EDAX). A second goal of the present work is to determine the extent to which homogeneous dissolution and precipitation of quartz can account for the observed permeability reduction by applying the kinetic equations for these processes [Rimstidt and Barnes, 1980] to our experimental system. Calculations of the silica content of discharged fluids are also compared with measurements from experiments NWD 2200 and NWD 2100 [Moore *et al.*, 1983]. NWD 2100 (called W250 by Moore *et al.* [1983]) was a permeability experiment on Westerly Granite under slightly different conditions than NWD 2200 (Table 1). Although we have not made SEM observations of the NWD 2100 sample, we include this experiment in the discussion section of the present paper because it provided data for comparison with the calculations of silica content of discharged fluids mentioned above.

#### PERMEABILITY EXPERIMENTS

The intact sample of Westerly Granite used in experiment NWD 2200 was 7.62 cm in diameter and 8.89 cm long, with a 1.27-cm central borehole (Figure 1). In experiment NWD 2200 the pore pressure in the borehole was maintained 0.5 MPa higher than the pore pressure at the outer edge of the sample. Fluids passed through the sample in response to this applied pore pressure gradient. The fluid pumped into the borehole was deionized water. A gold-coated resistance heater was positioned within the borehole (Figure 1). The temperature measured by a thermocouple, also located in the borehole, was maintained at a constant 300°C by servocontrol of the heater. The axial temperature gradient in the borehole of the sample was less than 2°C.

The procedure for determination of permeabilities in samples subjected to a temperature gradient is detailed in several publications [Morrow *et al.*, 1981; Moore *et al.*, 1983]. Briefly, the flow rates are determined by measuring the volume of water pumped into the borehole during an experiment. Permeabilities are calculated from the flow rates and the pore pressure gradient using Darcy's law. Permeability

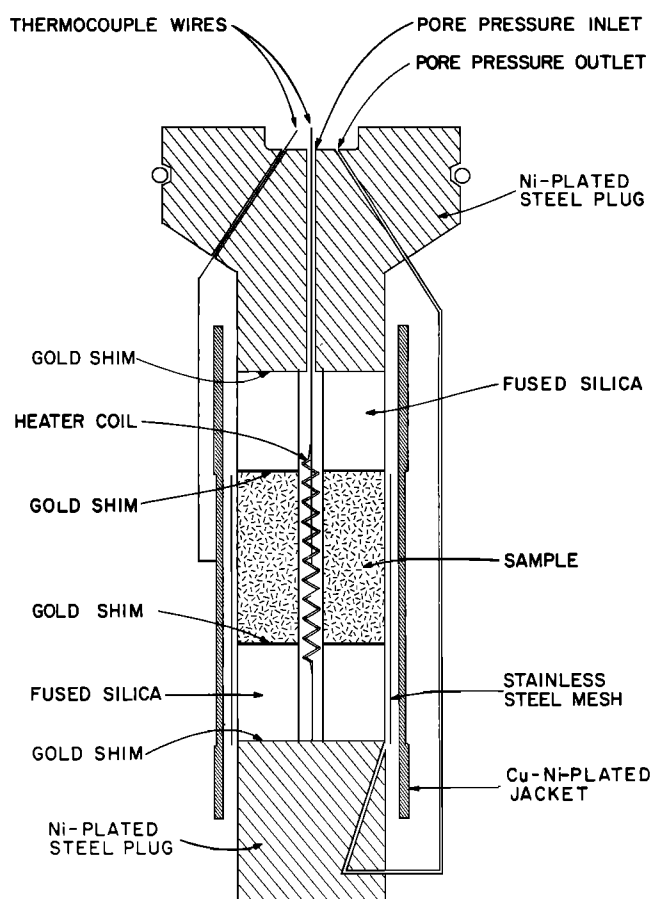


Fig. 1. Schematic of the sample assembly, showing an intact Westerly Granite cylinder as used in experiment NWD 2200.

data for the NWD 2100 and NWD 2200 experiments are listed in Table 1 and the chemical data are listed in Table 2. Permeability is plotted against time from the initial heating for NWD 2200 in Figure 2. All of these data have been published previously by Moore *et al.* [1983].

#### SCANNING ELECTRON MICROSCOPY

Samples from experiment NWD 2200 and the starting material were examined in a scanning electron microscope (SEM) equipped with an energy dispersive X ray detector. A cylindrical butt of the starting material and two butts of the altered sample (taken from cores cut parallel to the sample axis) were ground and highly polished with a series of alumina powders with grit sizes down to  $1\ \mu\text{m}$ , followed by a final polishing with  $0.3\ \mu\text{m}$   $\text{Ce}_2\text{O}_3$ . The final surface preparation for all of the butts consisted of ion beam thinning, which removes the damaged layers from the surface produced by the grinding and polishing procedure [Sprunt and Brace, 1974]. Because Sprunt and Brace [1974] found that significant topography developed for thinning times greater than 6 hours, obscuring the original features of samples, our samples were thinned for 5 hours.

In addition to these samples, two crack sections [Simmons and Richter, 1976] were prepared from the altered sample for both optical and SEM examination. Crack sections are about  $150\ \mu\text{m}$  thick, as compared to  $30\ \mu\text{m}$  for standard thin sections. The crack sections were polished on both sides, using a range of diamond pastes from 6 to  $1\ \mu\text{m}$  and a final polish with  $0.3\ \mu\text{m}$  alumina. Although these crack sections

were not ion-milled, their polished surfaces provided satisfactory SEM images, with the crack fillings showing only minor disturbance by the polishing procedure.

Detailed SEM observations were then made on the prepared butt of the Westerly starting material and on three areas of the two butts of the altered sample. These areas were located approximately 0.5 mm from the outer edge, 1 mm from the central borehole, and 5 mm from the central borehole (Figure 3). The area immediately adjacent to the borehole and that nearest the outer edge were chosen because they represent the two extremes with regard to temperature in the samples. The area located 5 mm from the borehole was chosen because our initial kinetic calculations indicated that precipitation of quartz would be most rapid in this region of the sample. However, our later calculations indicated that the maximum precipitation rate occurred at about 3 mm from the borehole. These calculations are discussed in detail in the appendix. A mosaic of overlapping SEM micrographs covering an area of  $5\ \text{mm}^2$  ( $100\times$ , about 20 grains) was constructed for each of the three locations in the altered sample. Mosaics are a useful way to map the cracks in an area consisting of several grains because they provide a better statistical sample than may be obtained from isolated micrographs. An attempt was made to choose areas that were as representative as possible, given the constraints of the relatively coarse grain size and the many different types of grain boundaries present among the various minerals. Specific locations along intragranular cracks and grain boundaries were chosen on these mosaics for examination at much higher magnification.

The SEM could also be operated in a mode in which an image was formed by collecting electrons emitted from the sample at high angles to the surface. This mode, called backscattered electron imaging (BSE) is sensitive to the mean atomic number in an area, making it possible to identify minerals based on differences in the intensity of the backscattered radiation. In addition to the SEM mosaic, a similar mosaic of BSE micrographs was constructed for each of the areas chosen. Both grain boundary cracks (defined as those cracks which are coincident with grain boundaries) and intragranular cracks were more readily identifiable in the BSE mode at relatively low magnifications (less than  $500\times$ ). Cracks of less than  $0.1\ \mu\text{m}$  width do not contribute significantly to permeability, based on the distribution of crack widths [Brace, 1977] and we therefore examined those larger cracks visible at magnifications of  $100\times$  in the SEM. In the following observations, we utilize the terminology of Simmons and Richter [1976] regarding cracks.

#### OBSERVATIONS

##### Starting Material

A fresh sample of Westerly Granite was examined in order to help distinguish between features that were initially present in the rock and those that were formed as a result of the experiment. These observations also permitted a qualitative comparison of the starting material with Westerly Granite samples studied by Sprunt and Brace [1974] and Hadley [1976]. Crack characteristics of the starting material are generally consistent with their observations, with the exception of some transgranular cracks that were present in our sample. Transgranular cracks are those intragranular cracks which meet two grain boundaries. Such cracks are present in

TABLE 2. Chemical Analyses of Discharged Fluids

Time, days	pH	SiO <sub>2</sub>	Na	K	Mg	Ca	HCO <sub>3</sub>	SO <sub>4</sub>	F	Cl	Balance, %
<i>NWD 2100</i>											
1.0	6.8		34	13	3.9	53		18	3.5	82	
1.9	7.1	210					130	17	3.4	61	
3.1	7.0	230					120	12	2.9	48	
3.3	6.7	160	32	11	2.9	38		12	3.0	49	
5.0	7.6	250	27	9	2.1	37		9	2.6	36	
8.9	7.2	180	28	7.6	1.9	31		7	3.2	21	
11.9	7.7	180					140	7	3.7	19	
<i>NWD 2200</i>											
1.0	7.6	47	62	32	4.4	91	300	36	3.8	91	-5.6
3.1	7.6	59	76	33	6.4	87	340	66	3.6	87	0.2
3.9	7.2	58	81	36	6.1	77	320	66	3.3	77	-4.9
4.9	7.0	69	81	37	7.5	73	350	70	3.5	73	5.6
8.0	7.6	34	78	41	6.8	64	320	60	3.6	64	4.8

Values are in milligrams per liter except as noted.

some of the smaller grains, especially quartz, and have maximum lengths of about 300  $\mu\text{m}$  in the 5 mm<sup>2</sup> area examined. Cracks which pass from one grain into another, called intergranular cracks, are very scarce.

Most intragranular cracks in the starting material are open; that is, the crack faces are separated and the cracks do not contain a filling material. However, such cracks are sometimes filled along short portions of their length, in which case the filling material is referred to as a bridge (Figure 4a). Crack bridges were first observed by *Sprunt and Brace* [1974] in Westerly Granite.

The grain boundaries between the two feldspars are almost always uncracked (Figures 5a and 6a). However, about 50% of the grain boundaries between quartz grains and between quartz and feldspar are cracked. The grain boundary cracks are about the same length as the diameter of quartz grains.

Pores are present in all three of the major phases. They are most abundant in plagioclase, less abundant in K-feldspar and least common in quartz (Figures 4a and 5a). The maximum pore width is about 10  $\mu\text{m}$ . The pores present in plagioclase occur preferentially in distinct compositional zones. In places where intragranular cracks run through the

zones of high pore density the crack surfaces are rough, but generally, the intragranular crack surfaces are smooth.

#### After Hydrothermal Fluid Flow

*General features.* The crack density in the altered sample is greater in the area near the outer edge of the cylinder than in the two areas close to the borehole. Fillings occur in many of the cracks in all three areas. However, important differences exist in the texture and local distribution of the fillings in the three areas.

Crack dimensions are of fundamental importance in determining the crack porosity of a rock and, thereby, the permeability. The arithmetic mean of crack widths near the borehole, near the outer edge and in the starting material, are 0.3, 0.4, and 0.4  $\mu\text{m}$ , respectively. Therefore no significant variation in crack width occurs among these samples. In addition to intragranular cracks and grain boundary cracks there are also intergranular cracks which pass through grain boundaries.

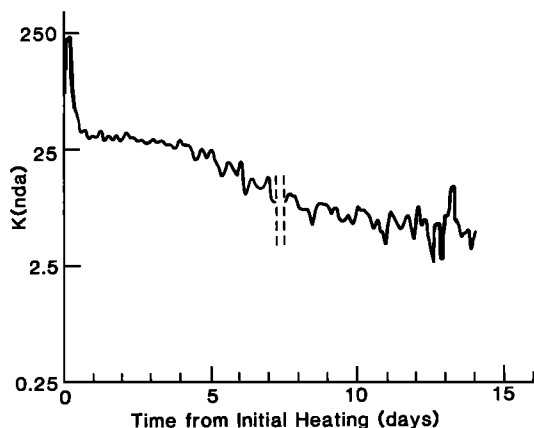


Fig. 2. Permeability (1 ndarcy =  $9.87 \times 10^{-21} \text{ m}^2$ ) as a function of time from initial heating for experiment NWD 2200. The vertical dashed lines represent a time when the pore pressure fluid pump was being recharged. Some anomalous peaks occur at times when fluid was withdrawn for chemical analyses.

#### AREAS OF SEM STUDY

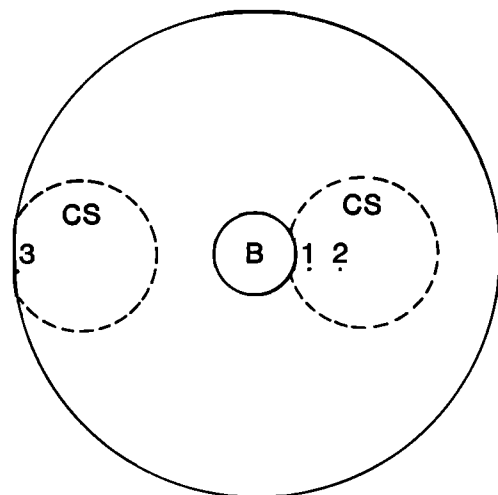


Fig. 3. Locations of areas of the altered sample that were studied in detail. The large solid circle represents the outer surface of the cylindrical sample and B designates the borehole. Crack sections were made from the areas within the dashed circles marked CS. The numbers designate the three areas studied.

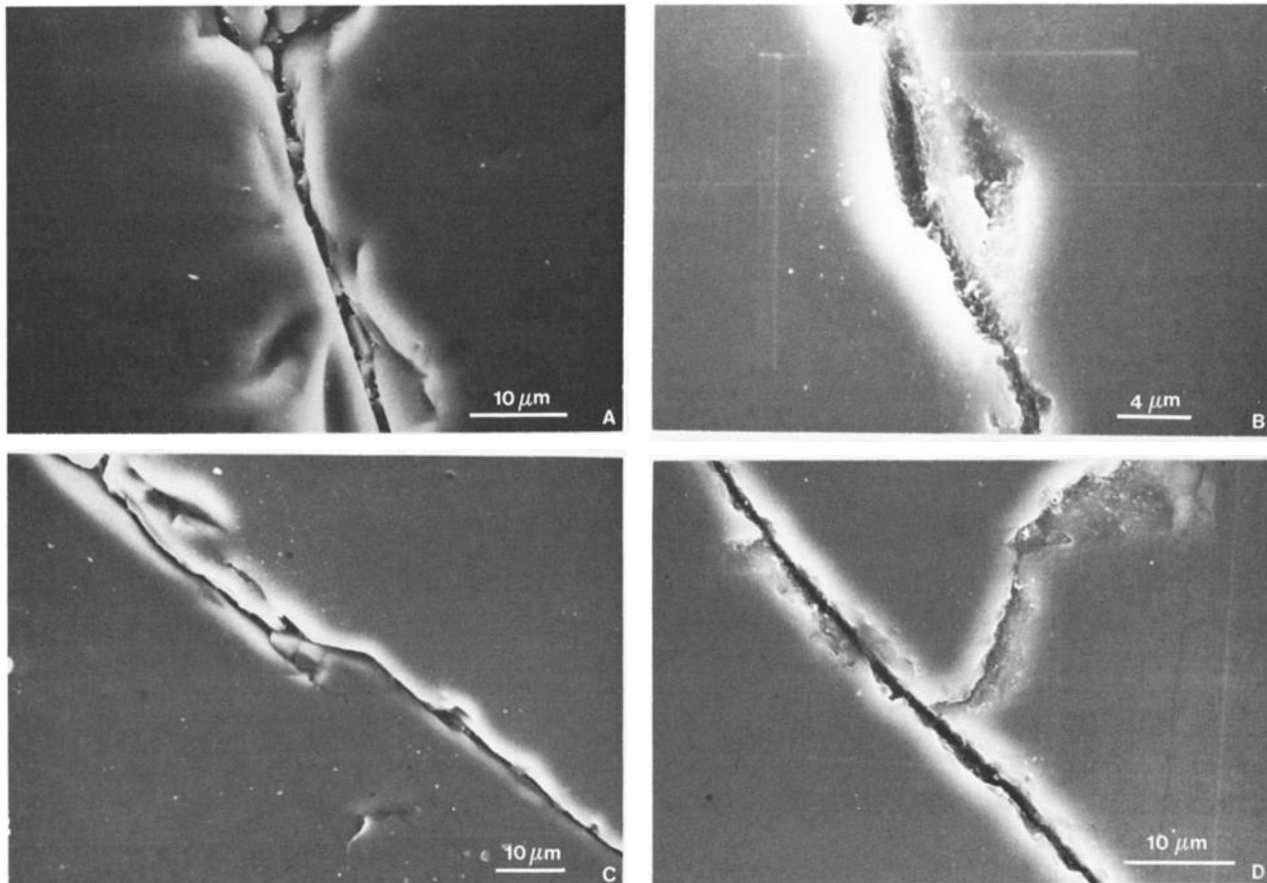


Fig. 4. Intragranular cracks in quartz (all SEM). (a) Starting material, crack containing isolated silica-rich bridges. (b) NWD 2200, 0.5 mm from outer edge. Note the variation in crack width and the presence of filling. (c) NWD 2200, 1.0 mm from borehole. Open cracks like this one are common near the borehole. These cracks contained fewer silica bridges than the starting material. (d) NWD 2200, 5.0 mm from borehole. Open cracks like this one are not as common here as in the area immediately adjacent to the borehole. Note also the somewhat rougher crack surfaces than in the starting material.

**Intragranular cracks: Quartz.** The quartz grains in sample NWD 2200 contain the highest density of intragranular cracks. Several large intersecting cracks form a loose network which connects the grain boundaries in most quartz grains (Figure 7). These cracks are easily distinguishable in both the petrographic microscope and  $100\times$  SEM micrographs, making it possible to correlate optical and SEM observations. As quartz grains tend to occur in clusters, the intragranular cracks are intimately associated with grain boundary cracks, and in the SEM it is difficult to distinguish large intragranular cracks from cracked grain boundaries (Figure 7). However, it was possible to make this distinction by examining the same areas in crack sections in a petrographic microscope. Intragranular cracks have been identified and marked in Figure 7 with small arrows. The unmarked cracks in Figure 7 are grain boundary cracks.

The length of intragranular cracks ranges from the diameter of a pore (a few microns) up to the grain size (several hundred microns, Figure 7). The outer edge of the altered sample has a higher density of transgranular cracks than does the starting material. However, the density of transgranular cracks in the two areas of the altered sample near the borehole appears to be lower than in the starting material. The intragranular cracks in the starting material (Figure 4a) and those in the two areas near the borehole (Figures 4c and 4d) are similar in size and appearance.

However, cracks near the outer edge of the altered sample usually contain a filling (Figure 4b) and therefore have a different appearance from intragranular cracks in the starting material. The width of the large intragranular cracks in the starting material and in all three areas of the altered sample ranges from 0.1 to  $1.0\ \mu\text{m}$ , neglecting the presence of filling (Figure 4). The walls of the larger cracks in the altered sample have a high degree of surface roughness, especially near the outer edge, making it difficult to estimate their width accurately (Figure 4b). In isolated places the intragranular cracks are highly curved, but generally, they are straighter than grain boundary cracks (Figure 7, area marked A).

In addition to large intragranular cracks, many smaller cracks are present which are not observable at a magnification of  $100\times$ . Near the outer edge of the altered sample, pores are often present along the intragranular cracks in quartz. The density of pores along cracks is higher than the density of isolated pores within the grains. Linear arrays of pores with no crack connecting them are rare in quartz although some of these connecting cracks were effectively closed. A gradation exists between the rough surfaces of large cracks as in Figure 4b and clearly separated pores. Apart from this increased density of pores along cracks, there is no difference in pore structure as compared to the starting material.

**Intragranular cracks: Feldspar.** Large intragranular

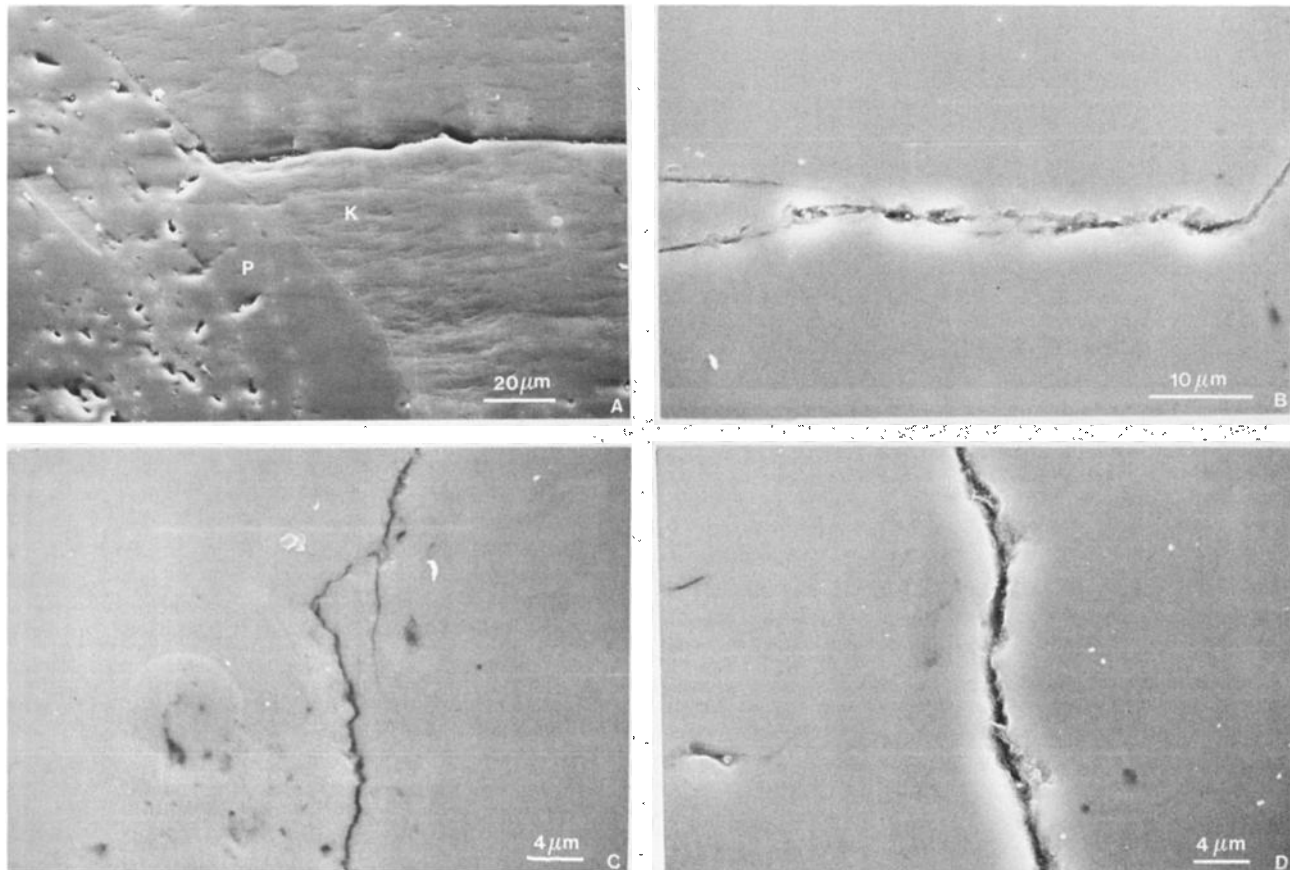


Fig. 5. Intragranular cracks in the feldspars (all SEM). (a) Starting material, an intragranular crack in K-feldspar adjoins an uncracked K-feldspar (K)/plagioclase (P) grain boundary. (b) NWD 2200, 3 mm from outer edge, crack in K-feldspar has associated pores. (c) NWD 2200, 1 mm from borehole crack in K-feldspar is narrow and sinuous with no filling. (d) NWD 2200, 5 mm from borehole, crack in K-feldspar contains a filling. This area has a very low pore density compared to the plagioclase.

cracks in the feldspars are generally similar to those in quartz, although they are somewhat less numerous and have widths of as much as a few microns (Figure 5a, K-feldspar grain). The intragranular cracks in feldspar of the starting material have a high surface roughness that is related to the high density of pores, particularly in plagioclase. In places where the intragranular cracks intersect pores, the crack surface is scalloped (Figure 5b). Pore density in K-feldspar is lower than in plagioclase, and correspondingly, there is less crack surface roughness. Otherwise, intragranular cracks in the two feldspars are similar. Surface roughness appears to be increased as a result of the experiment because pores occur more frequently along intragranular cracks in the altered sample (Figure 5b) than in the starting material (Figure 5a). In this regard, the behavior of the feldspars is similar to that of quartz. The feldspars also contain both open and filled cracks in all three areas (Figures 5c and 5d).

The grain size of the feldspars is larger than that of quartz, but the maximum crack length is about the same (300  $\mu\text{m}$ ). Thus the feldspars contain fewer transgranular cracks. Cleavage cracks occur in the feldspars, and are usually restricted to the interiors of grains. Such cracks are narrower than the other intragranular cracks. The cleavage cracks also are distinguishable by their orientation and lack of curvature.

*Grain boundary cracks.* Simmons and Richter [1976] classified grain boundary cracks as coincident, that is, fol-

lowing the grain boundary, or noncoincident, occurring within a single grain and intersecting a grain boundary. The altered sample contains arrays of intersecting, transgranular cracks which form networks by meeting cracked grain boundaries (Figure 4b). Such transgranular cracks are especially prevalent in quartz. Because these intragranular cracks meet grain boundaries, they might be classified as noncoincident grain boundary cracks [Simmons and Richter, 1976]. However, the question of whether these cracks are specifically related to the grain boundary is difficult to answer. In discussing grain boundary cracks, we refer only to the coincident grain boundary cracks.

Most of the grain boundaries between feldspars in the starting material were closed (Figure 6a), and they have remained closed during the experiment in all three areas examined (Figures 6b, 6c, and 6d). Out of 10 locations examined along different K-feldspar/plagioclase grain boundaries in the altered sample, only one grain boundary appeared cracked. The grain boundaries between quartz and the feldspars and those between quartz and the minor minerals in the altered sample are frequently cracked. However, the data are insufficient to determine whether a significant difference exists between the altered sample and the starting material in this regard. The grain boundaries between quartz grains were often cracked in the altered sample and the interconnection of these cracks with intragranular cracks forms a network that is generally not present in

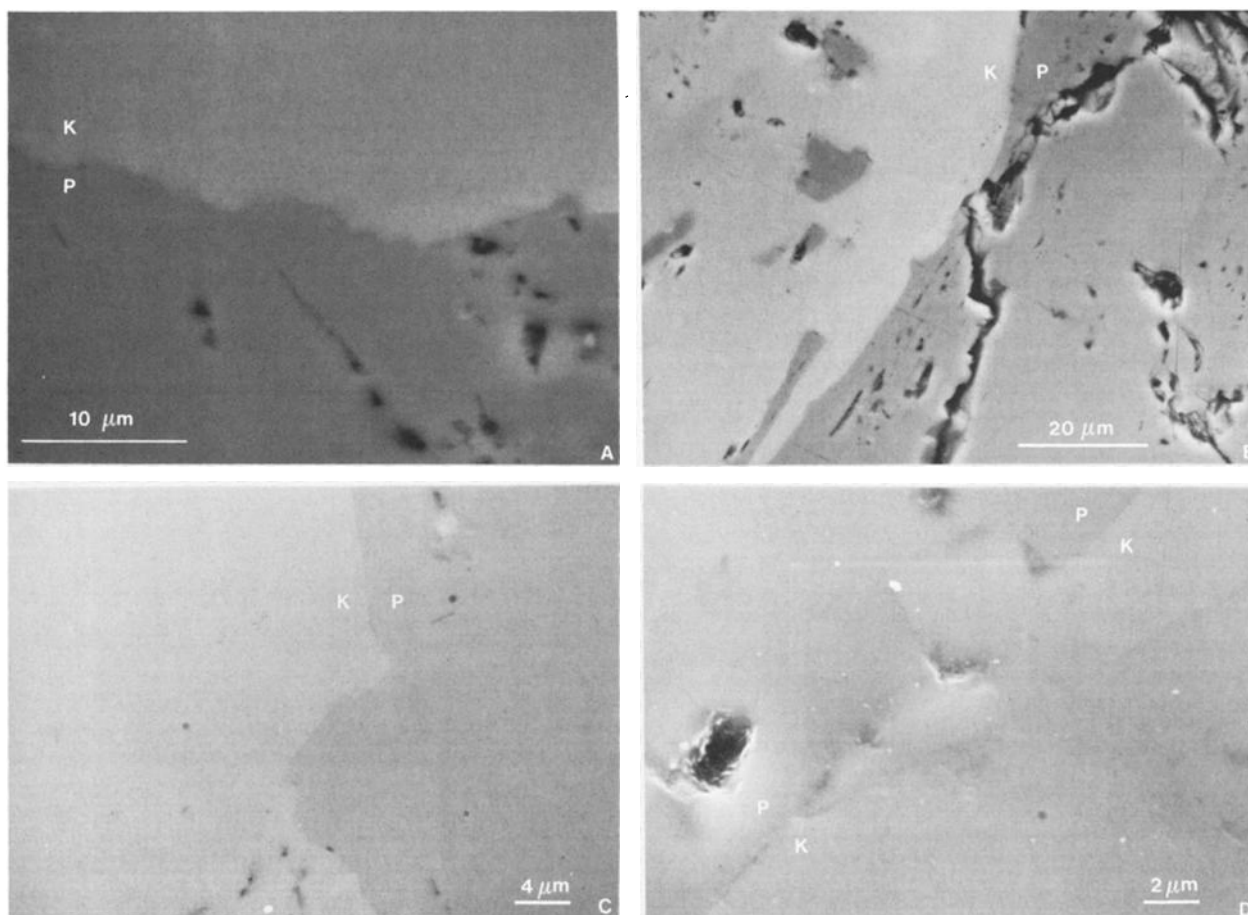


Fig. 6. Plagioclase/K-feldspar grain boundaries. (a) Starting material (BSE). (b) NWD 2200, 1 mm from outer edge. A large open crack is present in plagioclase but does not follow the grain boundary (BSE). (c) NWD 2200, 1 mm from borehole (BSE). (d) NWD 2200, 5 mm from borehole (SEM).

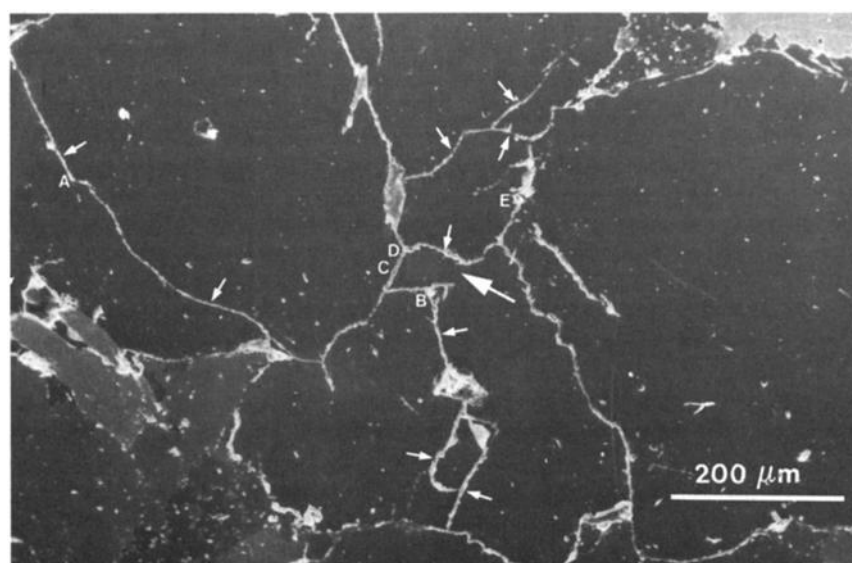


Fig. 7. NWD 2200, 0.5 mm from outer edge. A network of large intragranular cracks and grain boundary cracks in quartz (crack section, SEM). The intragranular cracks are marked with small arrows; all other visible cracks follow grain boundaries. A large arrow points to a place where an uncracked grain boundary exists for a short distance. The letters denote areas in which higher magnification micrographs were prepared. Some of these are shown in Figure 8.

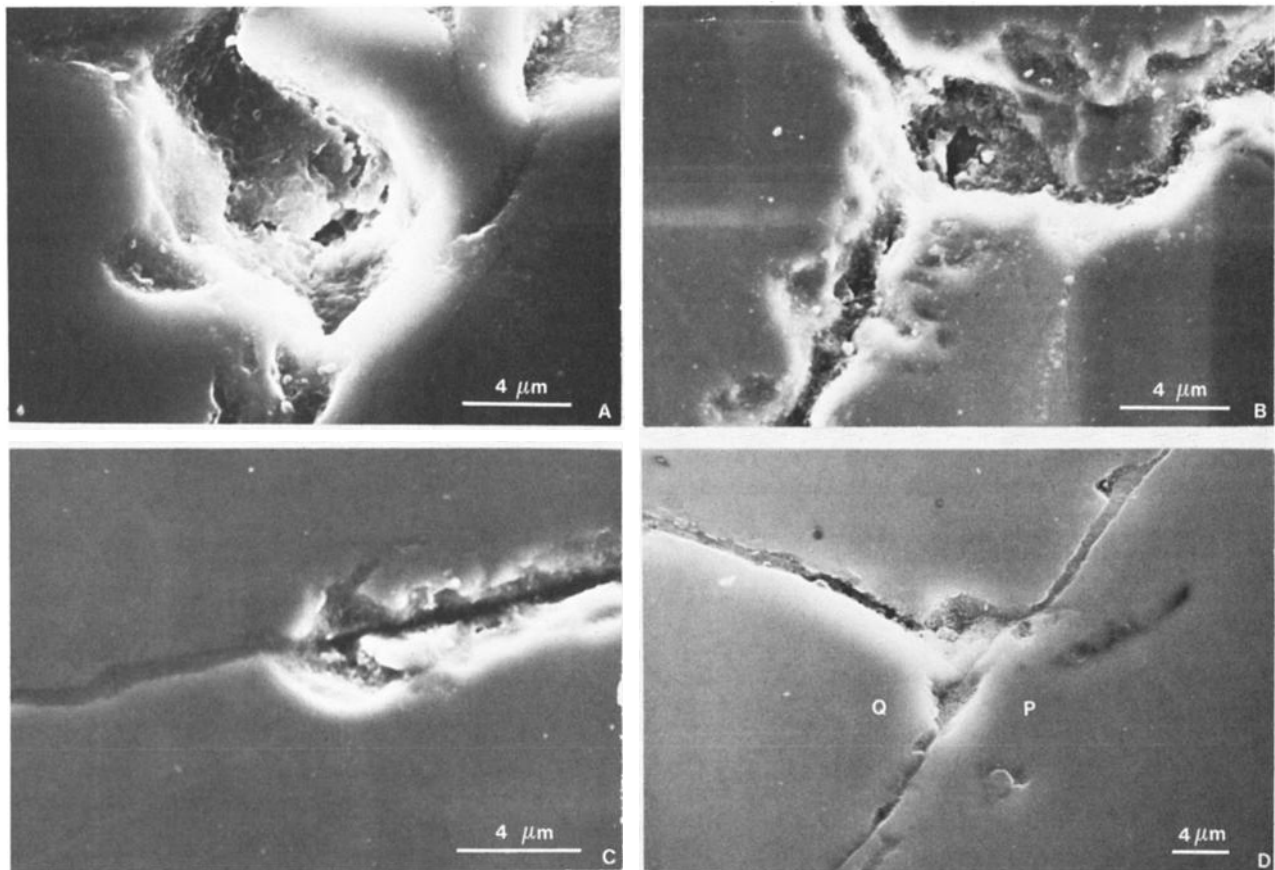


Fig. 8. NWD 2200, crack fillings (all SEM). (a) 0.5 mm from outer edge. Pore associated with grain boundary crack marked E in Figure 7. The platy filling is topographically lower than the polished surface surrounding the pore. (b) Intersection of grain boundary and intragranular cracks marked D on Figure 7. The platy filling contains a hole to a cavity underneath (the dark area in the center of the micrograph). (c) 1 mm from the borehole. Intragranular crack in quartz contains a massive silica-rich filling along a portion of its length. (d) 5 mm from the borehole. An intersection of a grain boundary crack between quartz (Q) and plagioclase (P), and an intragranular crack in quartz. There is a Ca-rich filling along both cracks, and a portion of the intragranular crack is open. The EDAX analysis indicated a significantly higher concentration of calcium relative to other elements than occurs in the plagioclase.

feldspar (Figure 7). The grain boundaries are only rarely interpenetrating.

**Crack filling: General.** SEM observations on the altered sample indicate that most cracks are filled along some portion of their length; however, there is a large variability in the amount of filling present, both for cracks near the borehole and near the outer edge. Due to this variability we were not able to determine quantitatively the fraction of cracks that are filled. Cracks in an area of quartz grains near the outer edge of the specimen are predominantly filled (Figures 4b, 8a, and 8b), whereas more than half of the total crack length examined in the area nearest the borehole is open (Figures 4c, 8c, and 8d). The area located 5 mm from the borehole appeared to have a somewhat greater fraction of filled cracks than the area 1 mm from the borehole (Figure 4d). However, a greater percentage of open cracks occurs in the area 5 mm from the borehole than near the outer edge.

**Crack filling: Outer edge.** Stereo pair SEM micrographs taken at crack intersections near the outer edge indicate that the filling material is not massive but consists of a series of plates separated by cavities. The stereo pairs were especially important in identifying holes in the filling and determining topographic relations between the filling in the cracks and

that in the crack intersections. Stereo pair SEM micrographs were prepared for areas shown in Figures 8a and 8b. Large, partially filled pores are present along some cracks in quartz (Figure 8a). The filling in the pores in Figure 8a has a platy appearance with a hole opening into a cavity underneath the top layer. This plate-and-void structure is not apparent within cracks except in the associated pores where the crack width increases to several microns (Figure 8a). In the crack intersection in Figure 8b the filling is platy and topographically lower than the filling in the adjacent cracks. In the center of Figure 8b there is a dark area which, in the stereo view, is seen to be a hole through the uppermost layer of filling material to a cavity that also contains some platy crystals.

The composition of the fillings in some of the cracks was determined by EDAX. There is considerable uncertainty regarding any quantitative assessment of the filling composition by this technique due to the unknown contributions of adjacent grains to the spectra. To minimize the effects of this complication, most of the spectra were obtained from fillings in quartz. However, we do not presume that the compositions of crack fillings in minerals other than quartz are necessarily the same as those for nearby quartz. In fact,

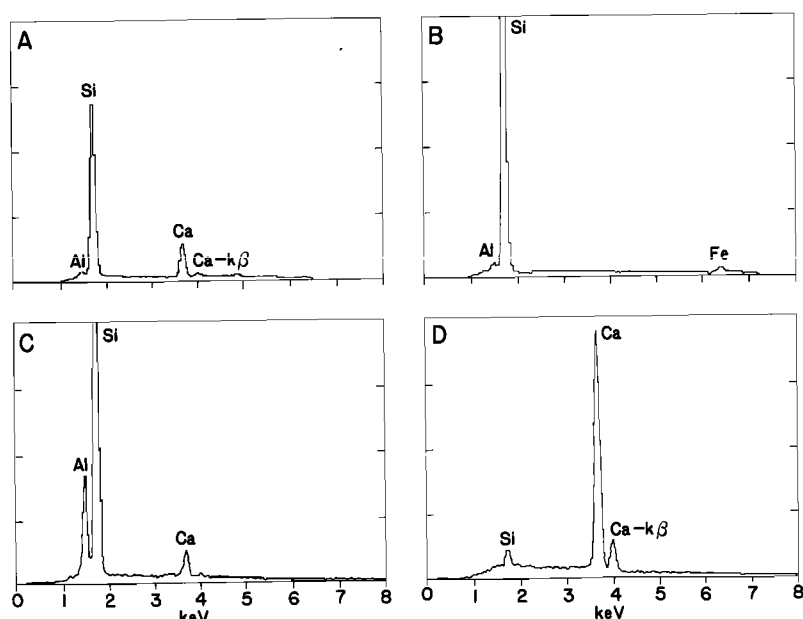


Fig. 9. NWD 2200, energy dispersive X ray spectra from cracks in quartz: (a) and (b) Cracks about 1 mm from the outer edge. (c) Massive filling in grain boundary crack, 1 mm from borehole. (d) Cracked filling with massive appearance similar to that of Figure 9c, 1 mm from borehole.

Morrow *et al.* [1981] found that mineral fibers on fractured surfaces had compositions that were specifically related to the mineral host.

The filling within the cracks near the outer edge of the altered sample is predominantly Si-rich (Figure 9b). In places, the filling contains some Ca and presumably Si as indicated by an energy dispersive X ray spectrum taken along a crack in quartz (Figure 9a). Sometimes Mn and/or Fe are present as minor constituents. In some areas, the cerium from the polishing compound was detected. The fact that a significant amount of aluminum was only once found in cracks in the samples polished with  $Ce_2O_3$  implies that the aluminum detected in many of the cracks in the crack sections came from the polishing compound. All the EDAX spectra in Figure 9 are from samples polished with  $Ce_2O_3$ .

**Crack filling: Borehole area.** Some cracks in the region immediately adjacent to the borehole have a massive filling. However, the filled cracks are frequently interrupted by open cracks (Figure 8c). These open cracks often have a drusy surface coating. The open cracks comprise at least 50% of the total crack length near the borehole (Figure 8c). This estimate does not take into account cracks that were too small to be observable in the  $100\times$  mosaic micrographs and also the possibility that some filled cracks near the borehole were not distinguishable from the grains themselves.

The filling in cracks from both areas near the borehole varies more in composition than the filling at the outer edge and usually has a massive appearance. Si-rich material containing both Ca and Al (Figure 9c) and an almost pure Ca filling (Figure 9d) are present. These two types of filling were found in the area 1 mm from the borehole within  $500\ \mu\text{m}$  of each other in neighboring quartz grains. Other quartz grains contained cracks with almost pure silica fillings. The Si-rich fillings in cracks near the borehole are often topographically at the same level as the polished surfaces of the grains (Figure 8c, filled portion).

## DISCUSSION

### Role of Cracks as Fluid Pathways

Low aspect ratio cavities (called cracks here) play an important role in establishing fluid pathways in Westerly Granite. Sprunt and Brace [1974] demonstrated that such cracks are generally open with some isolated silica bridges. The average length of the cracks is about 1/10 of the grain size [Sprunt and Brace, 1974]. This observation was confirmed by Hadley [1976], who also note that transgranular cracks are rare. The geometric mean crack width is  $0.2\ \mu\text{m}$  [Brace, 1977]. These observations suggest that a network of small intragranular cracks provides the interconnected porosity needed to make the rock permeable. Our observations of the starting material are consistent with the earlier work, with the exception of a greater density of transgranular cracks, particularly in quartz.

A fundamental problem regarding the definition of cracks arises when attempting to compare crack lengths in our altered samples with those determined by Sprunt and Brace [1974] and Hadley [1976] for the starting material. Hadley [1976] defined crack lengths to be those straight sections of open crack which were separated by at least three crack widths of filling (bridging material). Thus, by this definition the presence of crack bridges that are more than three crack widths long is an important limiting factor on crack length. Crack fillings in the altered sample would probably not be distinguishable from the original crack bridges. Conversely, in open cracks such as that shown in Figure 4c, the original crack bridges may have been dissolved. For either case, the estimate of crack length would be greater in the altered sample because one would have to presume that each straight portion of a crack is one crack length regardless of the presence or absence of filling. This indicates that the crack lengths determined by Sprunt and Brace [1974] and Hadley [1976] will be systematically lower than our measurements for the altered sample. Furthermore, Bruner [1984]

suggests that Hadley's technique of measuring crack lengths may result in an underestimate of crack length, which could also explain the discrepancy between measured and calculated  $p$  wave velocities found by Hadley [1976].

Thus comparison of our measurements of crack length with these earlier studies is complicated by the ambiguity in the definition of crack length. However, a greater density of transgranular cracks occurs at the outer edge of the altered sample than occurs in our sample of the starting material. This suggests that some cracks were introduced into the sample probably as a result of pressurization and/or heating. Thermal expansion of the fluid in existing cracks was probably the dominant factor in crack growth with anisotropic thermal expansion of minerals also a likely contributing factor. Of course, these thermal effects should be greatest near the borehole, but perhaps crack healing has caused the reduction of the crack density in this region. Alternatively, cracks near the borehole might contain a filling that was so similar to the neighboring grains that the cracks would not be visible in the SEM at the relatively low magnifications.

The intragranular cracks in quartz grains frequently intersect each other and the cracked grain boundaries (Figure 6). The feldspars exhibit a somewhat lower density of large, intragranular cracks and almost no cracks along grain boundaries with other feldspars. The grain boundaries between feldspars did not crack open during the experiment. Thus, during the early stages of the experiment the regions containing quartz should be substantially more permeable due to the difference in crack distribution. If the quartz forms continuous pathways through the rock, then the permeability is likely to be greater than if it occurs only in isolated clusters. Therefore the geometrical distribution of the major phases could be an important factor in determining the permeabilities of granitic rocks. In Westerly Granite the inhomogeneities in mineral distribution are on the scale of several grains; as a result, the crack distribution measured by Hadley [1976] may be biased if the area chosen was not representative. Because Hadley [1976] did not distinguish among the various minerals, potential effects of variations in the distributions of cracks cannot be ascertained from the statistics.

In addition to the low aspect ratio cracks, pores with roughly equal dimensions are present. In quartz and in K-feldspar these pores appear to be concentrated along cracks, in which case we identified them as being "associated with" the cracks. Such pores are often slightly elongate parallel to the plane of the crack (Figure 5b), which may indicate that they are actually cross sections through tubes. The observation that the density of pores "associated with" cracks is greater after the experiment suggests that some dissolution may have occurred along the cracks during the experiment. Pores are much more numerous in plagioclase than in quartz, making it difficult to distinguish those which may have formed during the experiment from those which were initially present along the cracks. We found only one instance of interpenetration of two grains along a grain boundary, which suggests that pressure solution [Robin, 1978] has not been significant in this sample. Rather, the evidence of dissolution is primarily the rough surfaces of cracks and the pores associated with cracks.

#### Calculation of Silica Concentrations Within the Samples

The filling material within cracks near the borehole varied in its texture from a minor drusy surface coating in the

majority of the cracks to a massive deposit. Both silica-rich and calcium-rich deposits occur as massive fillings in cracks near the borehole. The calcium-rich filling is probably calcite. The presence of calcite filling near the borehole is not surprising because the calcite that was replacing plagioclase in this region was much more etched than in the starting material [Moore et al., 1983]. This suggests that some of the calcite in the starting material dissolved during the experiment and may have been precipitated locally in the cracks. In natural hydrothermal systems both analcime and calcite have been found filling fractures in the same rock [Batzle and Simmons, 1976], an occurrence that was attributed to time-varying fluid chemistry. Our results indicate that two distinctly different types of filling, one silica-rich with possibly some Al and the other, apparently calcite, can be deposited under the same externally imposed conditions of confining pressure, temperature, pore pressure, and pore pressure gradient because both of these fillings occur in close proximity near the borehole. Despite these constant conditions, the composition of fluid discharged from the specimen varied with the flow rate and therefore time [Moore et al., 1983]. Also, the concentrations of some species increased or decreased steadily during the experiment while others exhibited maxima or minima. Any rationalization of these temporal variations must take into account the dilution of fluids discharged early the experiment by fluid existing initially in the space between the sample and the jacket. However, the variations of fluid composition in the latter portions of the experiments indicate that some temporal changes had been occurring in fluid composition within the samples. These various observations illustrate the complexity of chemical behavior of the fluids even under constant imposed conditions.

It is difficult to predict the composition of fluids within the sample because (1) the composition of the fluid entering the sample is not well known, and (2) the fluid composition within the sample changes as a result of dissolution and precipitation of minerals. The fluid being pumped into the borehole was deionized water. During its residence time in the borehole the silica concentration may have increased due to dissolution of quartz grains on the borehole surface. The extent to which this occurred is unknown, but a rough calculation of the silica concentration in the borehole using an estimated 5-day residence time gives 72 mg/L (based on rate equations of Rimstidt and Barnes [1980]). This is only about 12% of saturation at the temperature of the fluid in the borehole in NWD 2200 (300°C). We have been able to make these calculations only for quartz because rate equations of dissolution and precipitation of other minerals are not readily available.

The kinetics of quartz dissolution and precipitation reactions [Rimstidt and Barnes, 1980] may be used to determine the silica concentration of fluid within the sample, given some assumption of the starting composition within the borehole. Based on these calculations, the silica content of the fluid is plotted as a function of radius in Figure 10 for experiments NWD 2200 and NWD 2100. The calculation consisted of a numerical integration of

$$dm/dt = (A/M)(k_+ - k_-m) \quad (1)$$

where  $m$  is the molality of quartz in the solution,  $k_+$  and  $k_-$  are the dissolution and precipitation rate constants, and  $A/M$  is the ratio (area of reacting surface/mass of water). Details of the numerical technique are given in the appendix.

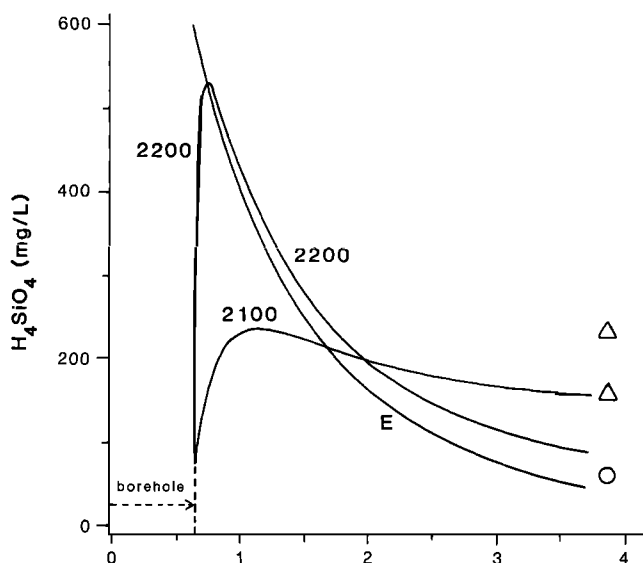


Fig. 10. These curves represent silica content of the fluid within the samples from experiments NWD 2100 (W250 from Moore *et al.* [1983]) and NWD 2200 (W300 from Moore *et al.* [1983]). The calculation is based on Rimstidt and Barnes' [1980] rate equations and is discussed in the appendix. The total fluid residence time was arbitrarily chosen to be that occurring 3 days after the initial raising of the temperature. The silica content is plotted as a function of radius in the samples. Measurements of the silica content of fluids discharged from NWD 2100 at 3.1 and 3.3 days are shown as triangles. The measured silica content for NWD 2200 at 3.1 days is shown as a circle. The equilibrium curve marked E is shown for comparison with the NWD 2200 curve only. The discrepancy between measured and calculated silica contents of the discharged fluids is discussed in the text.

For a low aspect ratio crack, the  $A/M$  ratio is inversely proportional to the crack width and therefore is directly proportional to the porosity. The initial crack porosities are  $1.2 \times 10^{-3}$  and  $0.9 \times 10^{-3}$  for NWD 2100 and NWD 2200, respectively. These numbers were obtained by adjusting the zero-pressure crack porosity ( $2 \times 10^{-3}$  [Brace *et al.*, 1968]) to account for the closure of cracks by the effective pressure. Since  $A/M$  is directly proportional to porosity, the  $A/M$  ratios also differ by a factor of 25% for these two experiments.

Due to the uncertainty in the measurements of crack width, we made calculations for  $A/M$  ratios of 3330 and 10,000 for the NWD 2200 experiment. These ratios correspond to crack widths of 1 and  $0.33 \mu\text{m}$ , respectively. For NWD 2100 the  $A/M$  ratios are lower by 25%. Even if the crack widths could be measured to an accuracy of, for example,  $0.1 \mu\text{m}$ , there would still be a significant difficulty in applying such measurements to the permeability problem. The difficulty arises because cracks which are both wider and longer are more likely to be components of active channel networks. Many of the small intragranular cracks measured by Hadley [1976] probably do not contribute to overall permeability. Therefore the effective  $A/M$  ratio should be biased towards lower values than that corresponding to the mean crack width.

For the simulation of the NWD 2200 experiment the initial silica content of the fluid was  $72 \text{ mg/L}$  based on calculations discussed above for an assumed 5-day fluid residence time in the borehole. This silica content is a high estimate because the 5-day residence time represents a high value for borehole

residence times occurring during this experiment. The silica content of the fluid increased very rapidly after it entered the sample, reaching saturation at  $521 \text{ mg/L}$  within 2 mm of the borehole. As the fluid moved outward beyond the point where saturation had occurred, precipitation of quartz began and the silica content decreased. Precipitation continued until the fluid reached the outer edge of the sample where the calculated silica content was  $85 \text{ mg/L}$  (Figure 10). Experiment NWD 2100 showed generally similar behavior, but the lower temperature and decreased residence time resulted in greater deviations from equilibrium in most regions of the sample. In particular, the maximum silica content was only  $232 \text{ mg/L}$ , whereas the final silica content was  $158 \text{ mg/L}$ . Thus the fluids discharged from the NWD 2100 sample would, on the basis of this calculation, have a greater silica content than those discharged from NWD 2200. In fact, this was observed, although the average silica contents of discharged fluids were  $50 \text{ mg/L}$  for NWD 2200 and  $210 \text{ mg/L}$  for NWD 2100. Therefore this particular model, with an  $A/M$  ratio of 2500 for NWD 2100, predicts the correct qualitative behavior and accounts for about 46% of the actual difference in silica concentrations (Figure 10). The second calculation of silica content for an assumed crack width of  $0.33 \mu\text{m}$  had results that were generally similar to those shown in Figure 10. However, for NWD 2100 the second calculation indicated a silica content of the discharged fluid of  $94 \text{ mg/L}$ . Since this is clearly a poorer fit to the data, we prefer the  $A/M$  ratio of 2500 (Figure 10).

One possible explanation of the difference between observed and calculated silica concentrations is that differences exist in the  $A/M$  ratio between the two experiments that are not simply caused by the closure of the cracks at the different effective pressures. For example, the surface area of crack faces could be changing during an experiment if the dissolution and precipitation processes are not homogeneous. In addition, the texture of crack fillings varies with temperature, suggesting that the different temperatures in the two experiments could have an effect on potential variations in the  $A/M$  ratio.

#### Model of the Crack-Sealing Mechanism

Variations in the silica contents of the fluids within the sample reflect dissolution or precipitation of silica and other silicate minerals in cracks. The crack porosity of the sample was therefore being changed locally due to these processes. In order to compute local changes in crack porosity the sample was divided into 40 hypothetical concentric cylinders. The net amount of quartz that was precipitated or dissolved in each cylinder was determined by simple summation. The cumulative effect of both dissolution and precipitation as a percentage of the initial crack porosity ( $0.9 \times 10^{-3}$ ) is shown in Figure 11 for conditions in the NWD 2200 experiment. The calculation of the amount of quartz precipitated in this experiment as a function of radius is similar to the calculation of the evolution of fluid compositions (Figure 10). Because fluid residence time changes during the experiment, the cumulative effect was determined by running small amounts of fluid through the hypothetical sample until the sum of these small amounts was equivalent to the total discharge from the actual sample. A new residence time was utilized for each increment of fluid that flowed through. Residence times were obtained from equation (A3) in the appendix with the flow rate  $Q$  calculated from a sixth-order

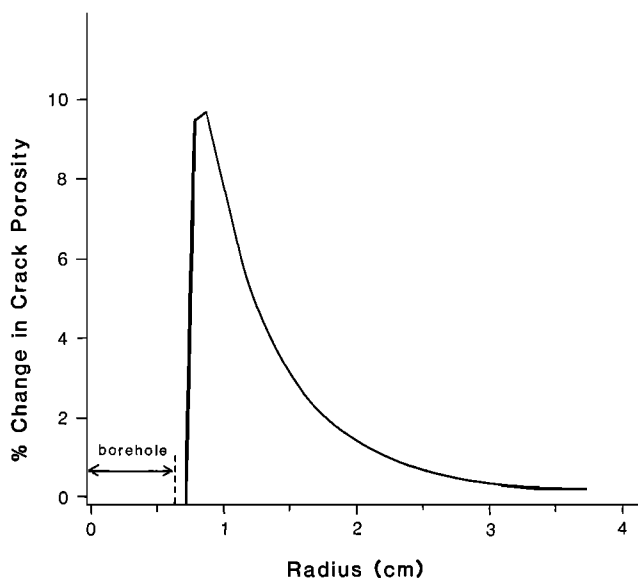


Fig. 11. This plot represents the amount of quartz deposited in sample NWD 2200 as a percentage of the available crack porosity. The calculation is based on *Rimstidt and Barnes'* [1980] rate equations with an assumed  $A/M$  ratio of 3330. The region of maximum deposition is located close to the borehole, but the amount of quartz deposited is less than 10% of the available crack porosity.

polynomial that was fitted to the data. A summation of the amount of silica dissolved or precipitated was maintained for each hypothetical concentric cylinder in the sample as the successive increments of fluid moved through. The result of this calculation is that in comparison to the crack porosity, very little material was deposited in the sample. The maximum deposition is about 10% of the crack porosity at a distance of 2 mm from the borehole (Figure 11). The effect of this deposit was estimated using

$$k = (m^2/A)\phi^3 \quad (2)$$

where  $k$  is permeability,  $m$  is hydraulic radius,  $\phi$  is crack porosity, and  $A$  is a constant. We assume that filling approximately 10% of the crack porosity will not change the hydraulic radius significantly. This assumption is valid if the precipitated quartz coats all of the cracks in the sample evenly because an even coating will be similar, in its effect on permeability, to the application of confining pressure. *Brace* [1977] has argued that for Westerly Granite the hydraulic radius is independent of effective confining pressure. Therefore the variation in permeability is proportional to the cube of porosity change. For the 10% maximum porosity change calculated for NWD 2200 the reduction in permeability is 27%. Thus this simple precipitation mechanism, in which quartz coats each crack uniformly, accounts for less than one third of the observed permeability reduction of 96%. Other factors that may be important in the permeability reduction are (1) crack healing, (2) precipitation in narrow sections of cracks causing a more rapid decline in permeability with decreasing porosity that is indicated by equation (2), (3) nonhomogeneous precipitation of quartz, and (4) nonhomogeneous precipitation of other minerals such as calcite and zeolites. Both of the last two possibilities are supported by our SEM observations. Any of the last three possibilities could result in the formation of discontinuous crack fillings which effectively seal the rock without

constituting a volumetrically significant portion of the crack porosity. However, we have not attempted to model such discontinuous crack closure.

#### CONCLUSIONS

During a permeability experiment in which heated water was forced through a cylindrical sample of Westerly Granite in a radial direction down a temperature gradient (300°C–92°C), the measured permeability dropped by a factor of about 25. The reduction of permeability in this experiment has been attributed to the dissolution and reprecipitation of minerals on crack surfaces [*Moore et al.*, 1983]. The work reported here focused on the crack characteristics of the sample and especially the crack fillings. Fillings in cracks in quartz immediately adjacent to the borehole consist of varying proportions of Ca and Si, along with a small amount of Al. Nearly pure silica fillings are common near the cooler, outer edge of the sample. Most cracks near the outer edge of the sample are filled, whereas at least 50% of cracks in the areas near the central borehole are open. The large cracks in quartz, whether open or filled, generally have rough surfaces and many have pores along them, suggesting that dissolution occurred at some point during the experiment. Some of this dissolution may have occurred during the initial heating when fluid residing in the sample was everywhere undersaturated.

The distribution of cracks in the sample is not completely homogeneous. Grain boundaries surrounding quartz are usually cracked open or have been cracked open at some time and subsequently filled. However, grain boundaries between the two feldspars are only rarely cracked open both in the starting material and in the intact altered sample. Thus the fluid pathways are more effectively connected in the regions containing quartz. The geometrical distribution of quartz is therefore important in determining the permeability of granitic rocks.

We developed a simple numerical integration routine to calculate the silica contents of fluid in the sample as a function of radius based on kinetic equations for silica dissolution and precipitation [*Rimstidt and Barnes*, 1980]. This calculation has a qualitatively correct result in that the silica content of the discharged fluid is greater in the run conducted at lower effective pressure and lower temperature. However, the variation in fluid residence time and temperature between the two experiments can account for only about 46% of the observed variation in silica content of the discharged fluids. An additional factor that may contribute to the observed variation is a potential change in the  $A/M$  (area of reacting surface/mass of water) ratio for cracks with time resulting in more efficient precipitation.

We have also calculated the total amount of silica precipitated in the samples based on *Rimstidt and Barnes'* [1980] rate equations. Calculations for NWD 2200 indicate that the maximum volume of quartz precipitated accounts for 10% of the crack porosity at a distance of 2 mm from the borehole wall. Utilizing a relation between crack porosity and permeability [*Brace*, 1977], we find that a simple solution-precipitation model of crack sealing, in which the precipitating quartz uniformly coats the cracks, can account for 27% of the observed 96% permeability reduction in the NWD 2200 experiment. One effect that could reduce permeability results from the texture of the material precipitated. The precipitates may have effectively closed off cracks by form-

ing bridges. Thus, even though the total amount of precipitated material might be small, the net effect on permeability could be large. Both the platy texture near the outer edge and the occurrence of open cracks interrupted by massive fillings near the borehole indicate inhomogeneous precipitation.

The discrepancy between the calculated and observed permeability reductions could also be caused by precipitation of quartz in narrow places along cracks. Also, the precipitation of calcite, which appeared to be greater in areas near the borehole, may have made important contributions to the permeability reduction. The precipitation of other minerals such as zeolites could be important, especially in the cracks in feldspars where locally higher Al concentrations may have occurred in the fluids. A fourth potential mechanism that could contribute to the observed permeability reduction is crack healing [Smith and Evans, 1984]. Evidence of crack healing is limited to the observation of a low crack density near the borehole. Crack healing in this region might reduce the connected crack porosity by the dissolution and reprecipitation of quartz on a local scale within cracks.

#### APPENDIX

The rate equation for dissolution and precipitation of silica [Rimstidt and Barnes, 1980] can be applied to calculate the changes in silica content of the fluid passing through the samples in our experiments. In the experiments the fluid changes temperature as it moves outward through the sample. Thus, in the calculations we have simulated the movement of the fluid through the sample by solving the rate equation for a fluid that is subjected to a series of temperature variations. For our calculations, temperature is expressed as a function of time rather than radius and is given by

$$T(t) = T_a + [(T_b - T_a)/\ln(b/a)] \ln\{(b^2 - a^2)(t/t_R) + a^2\}^{1/2}/a\} \quad (A1)$$

In this equation,  $T_a$  is the temperature at the borehole and  $T_b$  is the temperature at the outer edge;  $a$  and  $b$  are the borehole and outer edge radii, respectively;  $t_R$  is the total residence time for fluid in the sample given by

$$t_R = [2\pi h(b - a)^2 \ln(b/a)]/Q \quad (A2)$$

where  $h$  is the length of the sample and  $Q$  is the flow rate. The flow rates were calculated from the continuous record of the volume of fluid that had been pumped through the sample. These rates were fitted to a sixth-order polynomial to obtain a crude expression for the flow rate during an experiment.

The local changes in silica content of the fluid may be calculated from the rate equation

$$dm/dt = (A/M)(k_+ - k_-m) \quad (A3)$$

where  $m$  is the molal concentration of  $H_4SiO_4$  in solution,  $A/M$  is the ratio (area of reacting solid/mass of water), and  $k_+$  and  $k_-$  are the rate constants for dissolution and precipitation, respectively. Equation (A3) was obtained by Rimstidt and Barnes [1980] under the assumption that the activity coefficients  $a_{H_4SiO_4}$ ,  $a_{SiO_2}$ , and  $a_{H_2O}$  are all constant and are therefore included in the rate constants  $k_+$  and  $k_-$ . The  $A/M$  ratio can be calculated from an assumption of the crack width [Rimstidt and Barnes, 1980]. For the calculations

discussed here, the assumed  $A/M$  ratios vary from 2500 to 10,000.

Because the temperature is not constant in the sample and because the fluid is moving, the silica content of the fluid varies with radius and must be calculated numerically by integrating equation (A3). A Runge-Kutta technique is utilized for this calculation with the values of the two rate constants expressed as functions of time through equation (A1). For the calculation of the porosity change, the sample is divided up into a series of 40 concentric cylinders. The change in silica content of the fluid within each cylinder determines the amount of quartz deposited within that cylinder.

During each experiment a known amount of fluid passed through the sample. Because the total fluid residence time increased as the experiment progressed, the calculation of the amount of quartz deposited requires the total amount of fluid to be represented as the sum of small increments. Each of these increments corresponds to a particular global fluid residence time. The local changes in crack porosity are obtained in each hypothetical cylinder by utilizing the calculations mentioned above. The overall changes in crack porosity are obtained by a sum of the individual changes that occurred for each volume increment of fluid that passed through the sample.

#### REFERENCES

- Batzle, M. L., and G. Simmons, Microfractures in rocks from the geothermal areas, *Earth Planet. Sci. Lett.*, **30**, 71–93, 1976.
- Brace, W. F., Permeability from resistivity and pore shape, *J. Geophys. Res.*, **82**, 3343–3349, 1977.
- Brace, W. F., J. B. Walsh, and W. T. Frangos, Permeability of granite under high pressure, *J. Geophys. Res.*, **73**, 2225–2236, 1968.
- Bruner, W. M., Crack growth during unroofing of crustal rocks: Effects on thermoelastic behavior and near-surface stresses, *J. Geophys. Res.*, **89**, 4167–4184, 1984.
- Hadley, K., Comparison of calculated and observed crack densities and seismic velocities in Westerly Granite, *J. Geophys. Res.*, **81**, 3484–3494, 1976.
- Kharaka, Y. K., and I. Barnes, SOLMNEQ: Solution-mineral equilibrium computations, *Rep. PB-215 899*, 81 pp., Natl. Tech. Inf. Serv., U.S. Dep. Commer., Springfield, Va., 1973.
- Kranz, R. L., and J. D. Blacic, Permeability changes during time-dependent deformation of silicate rock, *Geophys. Res. Lett.*, **11**, 975–978, 1984.
- Madden, T. R., Random networks and mixing laws, *Geophysics*, **41**, 1104–1125, 1976.
- Montgomery, C. W., and W. F. Brace, Micropores in plagioclase, *Contrib. Mineral. Petrol.*, **52**, 17–28, 1975.
- Moore, D. E., C. A. Morrow, and J. D. Byerlee, Chemical reactions accompanying fluid flow through granite held in a temperature gradient, *Geochim. Cosmochim. Acta*, **47**, 445–453, 1983.
- Morrow, C., D. Lockner, D. Moore, and J. D. Byerlee, Permeability of granite in a temperature gradient, *J. Geophys. Res.*, **86**, 3002–3008, 1981.
- Rimstidt, J. D., and H. L. Barnes, The kinetics of silica-water reactions, *Geochim. Cosmochim. Acta*, **44**, 1683–1699, 1980.
- Robin, P.-Y. F., Pressure solution at grain-to-grain contacts, *Geochim. Cosmochim. Acta*, **42**, 1383–1389, 1978.
- Simmons, G., and L. Caruso, Microcracks and radioactive waste disposal, Scientific Basis for Nuclear Waste Management Symposium VI, *Mater. Res. Soc. Symp. Proc.*, **15**, 331–338, 1983.
- Simmons, G., and D. Richter, Microcracks in rocks, in *The Physics and Chemistry of Minerals and Rocks*, edited by R. Strens, pp. 105–137, Wiley-Interscience, New York, 1976.
- Smith, D. L., and B. Evans, Diffusional crack healing in quartz, *J. Geophys. Res.*, **89**, 4125–4135, 1984.
- Sprunt, E., and W. F. Brace, Direct observation of microcavities in crystalline rocks, *Int. J. Rock Mech. Min. Sci. Geomech. Abstr.*, **11**, 139–150, 1974.

Warren, N., Characterization of modulus-pressure systematics of rocks: Dependence on microstructure, in *The Earth's Crust: Its Nature and Physical Properties*, *Geophys. Monogr. Ser.*, vol. 20, edited by J. G. Heacock, pp. 119-148, AGU, Washington, D.C., 1977.

P. J. Vaughan, Department of Computer Sciences, Redcay Hall, State University of New York at Plattsburgh, Plattsburgh, NY 12901.

---

J. D. Byerlee, D. E. Moore, and C. A. Morrow, U.S. Geological Survey, 345 Middlefield Road, MS/977, Menlo Park, CA 94025.

(Received May 6, 1985;  
revised March 7, 1986;  
accepted March 10, 1986.)